ELSEVIER

PII: S0016-2361(98)00097-0

Fuel Vol. 77, No. 15, pp. 1705–1714, 1998

Printed in Great Britain
0016-2361/98 $19.00+0.00

The formation and destruction of NO in turbulent propane diffusion flames

Ph. Meunier, M. Costa* and M. G. Carvalho

Mechanical Engineering Department, Instituto Superior Técnico/Technical University of Lisbon, Av. Rovisco Pais, 1096 Lisboa Codex, Portugal

(Received 30 April 1998; accepted 11 June 1998)

This paper describes a study of the formation and destruction of NO in turbulent propane diffusion flames with recourse to both experiments and modelling. Detailed in-flame measurements of local mean gas species concentrations of O_2, CO, CO_2, unburnt hydrocarbons and NO_x and local mean gas temperature have been performed for three flames — two of them with the same Froude number and two with the same Reynolds number. These experimental data have been analysed with the aid of a mathematical model. For the NO calculations, three reaction schemes have been used: the Zeldovich reactions, an overall approximate prompt reaction, and a 27 reaction scheme, which includes the thermal NO and the prompt NO reactions and the NO to HCN recycle via fuel NO reactions. The main conclusions are that in the present flames: (1) the prompt NO (or Fenimore) mechanism is the dominant route for the NO formation; and (2) the reactions between NO and hydrocarbon radicals, recycling NO to HCN via the fuel NO reactions, play an important role in the global NO reduction.

(Keywords: nitrogen oxides; turbulent diffusion flames)

INTRODUCTION

The chemical reactions that describe the formation and removal of NO in hydrocarbon combustion are usually grouped into three mechanisms [1–3]: (i) the thermal NO mechanism; (ii) the prompt NO mechanisms; and (iii) the fuel NO mechanism. The thermal NO mechanism comprises the well-known extended Zeldovich reactions which represent the oxidation of atmospheric molecular nitrogen. The prompt NO mechanisms originate from the explanations given to the NO formed at a faster rate than that calculated from the thermal NO mechanism with the equilibrium assumption [2]. Three explanations have been given: O and OH atom superequilibrium concentrations, the N_2O mechanism and the Fenimore mechanism. In hydrocarbon diffusion flames, however, the Fenimore mechanism has been found to be dominant. This mechanism comprises a reaction sequence initiated by reactions between fuel radicals and nitrogen. Finally, the fuel NO mechanism consists of reactions describing the NO formation from the oxidation of the chemically bound nitrogen in the fuel and the NO destruction via the reactions between NO and fuel hydrocarbon radicals. These reactions recycle NO to HCN which, in turn, may react to form NO or N_2. They are here considered as the reburn NO reactions since no fuel N is initially present in the fuel.

The relative importance of the different NO mechanisms is a crucial issue to both reduce and model NO_x emissions from combustion equipment. In laminar hydrocarbon premixed flames, the thermal mechanism is the major source of NO under fuel-lean to stoichiometric conditions, while the prompt mechanism dominates under low-temperature and fuel-rich conditions [1,4]. Such conclusions do not hold for diffusion laminar flames owing to the importance of the interaction between mixing and chemical processes and the presence of both fuel-rich and fuel-lean zones. Comparisons between in-flame NO measurements and calculations performed in laminar methane diffusion flames showed that the NO formation is dominated by the prompt mechanism, which was responsible for more than two thirds of the total NO formed [4]. Previous measurements for the same type of flames had also shown that the NO, mainly formed outside the flame surface, penetrates it via convection–diffusion processes and that, inside this surface, about 80% of this NO is converted to N_2 or other nitrogen-containing species [5]. Recently, further evidence of the importance of the prompt NO and NO to HCN recycle (or reburn NO reactions) has been presented based on numerical studies in laminar methane diffusion flames [6–8].

The literature reveals that there is a lack of studies like those referred to above for turbulent hydrocarbon diffusion flames. The studies for turbulent flames have mainly been devoted to measurements of global NO_x emission indices which have been scaled with fluid mechanical parameters to evidence the main physical effects associated with the NO_x production [9–13]. In particular, the role of the thermal and prompt NO and of the reburn NO reactions has not yet been considered simultaneously in turbulent diffusion flames. As a consequence, the mathematical models used for these flames [13,14] have been restricted to both thermal and prompt

* Corresponding author. Tel.: +351-1-8417186; Fax: +351-1-8475545.

NO, whose formation rates were estimated from the Zeldovich reactions and an overall approximate prompt NO reaction [15], respectively.

The aim of the work reported here is to study the formation and destruction of NO in turbulent propane diffusion flames with recourse to both experiments and modelling. To this end, detailed in-flame measurements of local mean gas temperature and local mean gas species concentrations (O_2, CO, CO_2, unburnt hydrocarbons and NO_x) have been analysed with the aid of a mathematical model which considers the different NO reaction mechanisms.

EXPERIMENTAL METHOD

An overview of the test section is shown in *Figure 1*. It has been fully described previously by Meunier *et al.* [16]. The burner consisted of a straight tube through which the fuel jet was injected vertically into still air. Three different sized nozzles of 2.05, 3.25 and 4.15 mm i.d. were employed. Commercial propane (99.8% purity) was used. The flames were surrounded by a fine mesh wire screen constructed of movable 1×2.4 m^2 panels to minimise room disturbances. In the present experimental set-up no measures were employed to attach the flame to the nozzle, so that the measurements were performed in lifted flames, with lift-off heights up to 5 cm.

The sampling of combustion gases from the flame region for the measurement of local mean O_2, CO, CO_2, unburnt hydrocarbons (UHC) and NO_x concentrations was achieved using a water-cooled stainless steel probe [16]. A schematic of the gas analysis system is also shown in *Figure 1*. The analytical instrumentation included a magnetic pressure analyser for O_2 measurements, non-dispersive infrared gas analysers for CO, CO_2 and NO_x, measurements and a flame ionization detector for UHC (expressed as C_3H_8) measurements. Zero and span calibrations with standard mixtures were performed before and after each measurement session. The maximum drift in the calibration was within $\pm$ 2% of the full scale. In the flame region, the major sources of uncertainties in the concentration measurements were associated with the quenching of chemical reactions and aerodynamic disturbance of the flow. Quenching of the chemical reactions was rapidly achieved upon the samples being drawn into the central tube of the probe due to the high water cooling rate in its surrounding annulus — our best estimates indicated quenching rates of about 10^6 K/s. NO_2 removed within the probe and sampling system by acid formation was negligible. No attempt was made to quantify the probe flow disturbances. The repeatability of the gas species concentration data was, on average, within 10%.

Local mean gas temperature measurements were obtained using fine wire (25 μm) uncoated thermocouples of Pt/Pt:13% Rh. As flame stabilisation on the temperature probe was not observed, interference effects were unlikely to have been important and, hence, no effort was made to quantify them. The uncertainty due to radiation heat transfer was estimated to be less than 5% by considering the heat transfer by convection and radiation between the thermocouple bead and the surroundings.

The sample and the thermocouple probes were mounted on a 3D computer controlled traverse mechanism which allowed for axial and radial movements throughout the flame. The analogue outputs of the analysers and thermocouple were transmitted via an A/D board to a PC where the signals were processed and the mean values computed. No thermal distortion of any of the probes was observed and the positioning of the sample probe tip and the thermocouple junction in the flames was precise to within $\pm$ 0.5 mm.

MATHEMATICAL MODEL

Main flow and combustion equations

The mathematical model is based on a density-averaged form of the balance equations for mass, momentum and

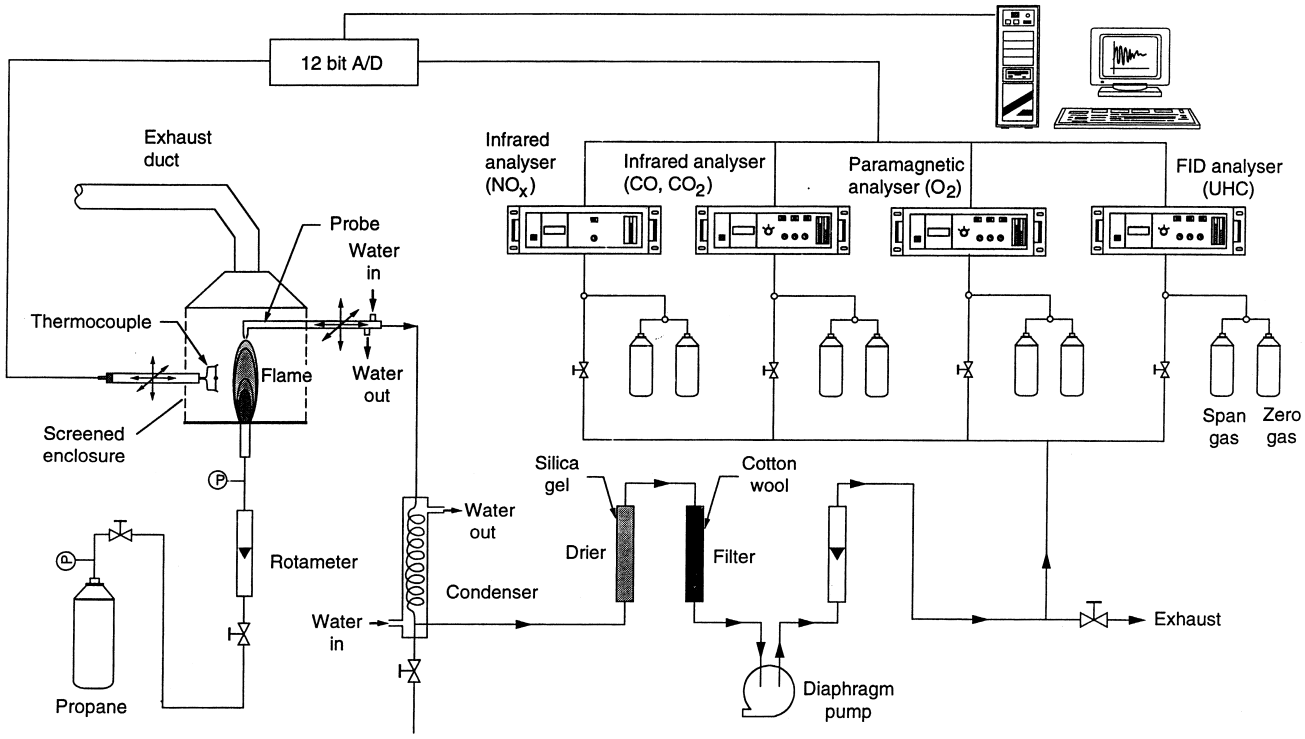

Figure 1 Experimental set-up

energy, and relevant scalar quantities describing turbulence and combustion. The set of equations is closed by the k–ε turbulence model using standard coefficients and no axisymmetric jet spreading correction. Buoyancy effects are taken into account in the momentum equation only. Combustion is modelled using the stretched laminar flamelet model and the assumed PDF method. The present flamelet approach considers a flamelet library consisting of two scalar profiles: one corresponds to undisturbed flamelet burning and the other to non-reactive mixing [17]. This means that the local structure in the turbulent flame is assumed to be determined by a combination of an unstretched laminar diffusion flame and the inert mixing between fuel and oxidiser streams. The latter occurs when the local stretch parameter, which is represented by the strain rate of the smallest eddies, exceeds a quenching limit [18]. The quenching value for the strain rate was taken equal to 565 s^{-1} [18], while the coefficient relating the strain rate value with the k–ε values was 0.16 [16]. For both flamelet burning and inert mixing scalar profiles, the instantaneous species mass fractions are related to the value of the mixture fraction. A linear variation of the species mass fractions with the mixture fraction is adopted for the inert mixing profile. The relationship between the mixture fraction and the species mass fractions for the flamelet burning profile is obtained from computations of an unstretched non-premixed propane flame [19]. The chemical mechanism considered involves the oxidation of propane into CO and H_2 by a single step. The subsequent CO and H_2 oxidation is represented by a scheme of 12 elementary reactions. The chemical species considered in this mechanism are C_3H_8, O_2, N_2, CO_2, CO, H_2O, OH, H_2, O and H. For the PDF calculation, the mixture fraction and the strain rate are assumed to be statistically independent. The probability of flamelet burning or non-reactive mixing to occur is calculated from the strain rate distribution which is assumed to be a quasi-Gaussian function [18]. The mean species concentration is then obtained with the aid of the probability density function of the mixture fraction. This is assumed to be a conditional clipped Gaussian function [20] which is calculated from the mean mixture fraction and its variance for which a transport equation is solved. The gas temperature is calculated from the enthalpy using well-known thermodynamic concepts. A piecewise linear relationship between the instantaneous values of enthalpy and mixture fraction is assumed following Abou Ellail *et al.* [21]. If there were no radiation losses this relationship would be linear. Therefore, for a given mixture fraction the difference between the enthalpy obtained from the linear adiabatic relation and the enthalpy given by the piecewise linear relationship corresponds to the radiation loss [22]. The radiation term of the energy equation is evaluated using the discrete transfer method [23] and considering CO_2, H_2O and soot as participating species. Correlations of gas total emittance, extended to account for soot particles, have been used [24]. A transport equation is solved for the soot mass fraction with a single step process being chosen for the soot formation rate [25] and the soot oxidation rate [26].

Nitric oxide calculations

Three nitrogen reaction schemes have been used in the present work to predict the mean NO concentration fields. The first one included the Zeldovich reactions — the thermal NO mechanism. The second reaction scheme used in the present study, herein referred to as the prompt NO mechanism, was an overall approximate prompt reaction initially proposed by de Soete from measurements carried out in nitrogen/ethylene/oxygen flames [15] and later modified by Williams and co-workers according to the type of fuel, the temperature range or the mixture strength [14]:

$$\frac{dX_{NO}}{dt} = kfX_{O_2}^{b}X_{N_2}X_{fuel}\exp\left(-\frac{60\,000}{RT}\right) \quad (1)$$

where X denotes the mole fraction, b the partial reaction order with respect to oxygen concentration being the activation energy expressed in cal/mol. The term f takes both the type of fuel and the air/fuel ratio effects into account:

$$f = 4.75 + C_1 n - C_2\phi + C_3\phi^2 - C_4\phi^3 \quad (2)$$

where n denotes the number of carbon atoms in the fuel and ϕ the equivalence ratio. C_1, C_2, C_3 and C_4 take the values of 0.082, 23.2, 32 and 12.2, respectively. Finally, the reduced nitrogen chemistry scheme proposed by Glarborg *et al.* [27] — herein referred to as the global NO mechanism — was used. It comprises 27 reactions accounting for both the thermal and the prompt NO mechanisms as well as NO to HCN recycling and conversion of HCN to NO or N_2. In the present study, the distinction between $^1CH_2$ and $^3CH_2$ considered by Glarborg *et al.* was not made. The reaction between HCCO + NO [1] was added. *Table 1* lists the reactions and the corresponding kinetic parameters.

The NO concentration fields are calculated by solving a transport equation for the Favre-averaged NO mass fraction. In the case of the global NO mechanism a transport equation for the Favre-averaged HCN mass fraction is also solved. The mean NO and HCN formation rates are calculated using the PDF method. The instantaneous formation rates are equal to zero when considering the inert mixing. For the flamelet burning, the instantaneous formation rates are obtained as a function of the mixture fraction from the flamelet data for major species and radicals. In addition, for the global NO mechanism, steady-state assumptions are used for obtaining the instantaneous concentrations of the other nitrogen-containing species (instantaneous NO and HCN mass fractions are assumed to be constant over the mixture fraction range) and fuel radicals involved in the NO chemistry. The concentration of these fuel hydrocarbon radicals is obtained using a simplified propane reaction mechanism [28,29]. In this scheme, C_2H_2 and CH_3 are assumed to be formed from propane, roughly at the rate of the reaction [29]:

$$C_3H_8 + H \rightarrow C_3H_7 + H_2 \quad (3)$$

which may be followed by the faster reactions:

$$C_3H_7 \rightarrow C_2H_4 + CH_3 \quad (4)$$

$$C_2H_4 + H \rightarrow C_2H_3 + H_2 \quad (5)$$

$$C_2H_3 \rightarrow C_2H_2 + H \quad (6)$$

to yield the overall process:

$$C_3H_8 + 2H \rightarrow C_2H_2 + CH_3 + 2H_2 + H \quad (7)$$

where CH and CH_2 are assumed to be consumed through reactions with virtually all species (except with N_2 for both CH and CH_2, and C-containing species for CH_2) at rates that are roughly the same so that one writes [29]:

$$CH + M' \rightarrow \text{products} \quad (8)$$

$$CH_2 + M'' \rightarrow \text{products} \quad (9)$$

where M′ denotes any molecule other than N_2 and M″ any

molecule not containing N or C atoms. The reactions are summarised in *Table 2*.

Numerical solution

The numerical solution was accomplished using a finite-volume technique, a fully elliptic solver and a staggered grid [30]. The main flow and combustion equations as well as the NO and HCN transport equations were integrated over each control volume and discretised using a finite-difference scheme. The central difference discretisation scheme was employed except for the convective terms which were discretised using the hybrid central difference/upwind scheme. Coupling between the pressure and velocity fields was handled by the SIMPLE algorithm and the sets of discretised algebraic equations were solved by the Gauss–Seidel line-by-line iterative procedure. A 42 × 42 node grid covering a calculation domain of 0.5 m × 1.5 m was used. A grid refinement was tested without improving the agreement between the predictions and the measurements shown below.

RESULTS AND DISCUSSION

Table 3 summarises the initial conditions for the three flames investigated. The flow conditions were varied by changing the initial velocity (u_0) and the nozzle exit internal diameter (d_0) in order to allow the confrontation of two flames with the same Froude number (Fr) — flames A and B — and two with the same Reynolds number (Re) — flames A and C.

Figures 2 and 3 show the measured axial profiles of local mean O_2 and CO_2 concentrations for flames A, B and C, respectively. It is seen that the profiles of flames A and B are similar in both figures. This similarity is also observed in the measured axial profiles of local mean C_3H_8 and CO concentrations for flames A and B [28]. These results indicate that the Froude number is the relevant fluid mechanical

Table 1 NO reaction mechanism [22]. Rate coefficients in the form $k_f = AT^b \exp(-E/RT)$. Units are mol, cm^3, K and cal/mol

	Reaction	*A*	*b*	*E*
1	$NH + H \rightarrow N + H_2$	3.0×10^{13}	0.0	0
2	$NH + O \rightarrow NO + H$	5.5×10^{13}	0.0	0
3	$NH + O \rightarrow N + OH$	7.0×10^{11}	0.5	0
4	$NH + NO \rightleftarrows N_2O + H$	1.2×10^{14}	− 0.3	0
5	$N + OH \rightarrow NO + H$	3.8×10^{13}	0.0	0
6	$N + O_2 \rightarrow NO + O$	6.46×10^{9}	1.0	6280
7	$N + NO \rightleftarrows N_2 + O$	3.31×10^{12}	0.3	0
8	$O + N_2 + M \rightarrow N_2O + M$	3.25×10^{8}	1.41	15340
9	$N_2O + H \rightarrow N_2 + OH$	7.6×10^{13}	0.0	15200
10	$HCN + O \rightarrow NCO + H$	1.41×10^{4}	2.64	4980
11	$HCN + O \rightarrow NH + CO$	3.47×10^{3}	2.64	4980
12	$HCN + OH \rightleftarrows CN + H_2O$	1.51×10^{15}	− 0.68	12380
13	$HCN + OH \rightarrow NCO + H_2$	5.5×10^{3}	2.67	10800
14	$CN + OH \rightarrow NCO + H$	$6. \times 10^{13}$	0.0	0
15	$CN + O_2 \rightarrow NCO + O$	1.0×10^{13}	0.0	0
16	$NCO + H \rightarrow NH + CO$	5.01×10^{13}	0.0	0
17	$NCO + OH \rightarrow NO + CO + H$	1.0×10^{13}	0.0	0
18	$NCO + NO \rightarrow N_2O + CO$	3.02×10^{17}	− 1.53	260
19	$CH + N_2 \rightarrow HCN + N$	4.37×10^{12}	0.0	22000
20	$C + N_2 \rightarrow CN + N$	6.31×10^{13}	0.0	46000
21	$CH_2 + NO \rightarrow H + HCNO$	1.39×10^{12}	0.0	− 1100
22	$CH + NO \rightarrow HCN + O$	1.10×10^{14}	0.0	0
23	$C + NO \rightarrow CN + O$	1.9×10^{13}	0.0	0
24	$C + NO \rightarrow N + CO$	2.88×10^{13}	0.0	0
25	$N + CO_2 \rightarrow NO + CO$	1.29×10^{12}	0.0	4950
26	$N + CH_3 \rightarrow HCN + H_2$	7.08×10^{13}	0.0	0
27	$HCCO + NO \rightarrow HCNO + CO$	2.0×10^{13}	0.0	0[a]

[a] Miller and Bowman [1]

Table 2 Propane reaction mechanism. Rate coefficients in form $k_f = AT^b \exp(-E/RT)$. Units are mol, cm^3, s, K and cal/mol

	Reaction	*A*	*b*	*E*	Reference
1	$C_3H_8 + H \rightarrow C_3H_7 + H_2$	1.8×10^{14}	0.0	8370	[29]
2	$CH_3 + H \rightarrow CH_2 + H_2$	9.0×10^{13}	0.0	15100	[29]
3	$CH_3 + OH \rightarrow CH_2 + H_2O$	7.5×10^{6}	2.0	5000	[29]
4	$CH_3 + O \rightarrow CH_2O + H$	8.0×10^{13}	0.0	0	[1]
5	$CH_3 + O_2 \rightarrow CH_3O + O$	2.05×10^{19}	− 1.570	29229	[1]
6	$C_2H_2 + O \rightarrow CH_2 + O$	1.02×10^{7}	2.0	1900	[29]
7	$C_2H_2 + O \rightarrow HCCO + H$	1.02×10^{7}	2.0	1900	[1]
8	$C_2H_2 + OH \rightarrow C_2H + H_2O$	3.37×10^{7}	2.0	14000	[1]
9	$C_2H_2 + OH \rightarrow HCCOH + H$	5.04×10^{5}	2.3	13500	[1]
10	$CH_2 + H \rightarrow CH + H_2$	1.0×10^{18}	− 1.56	0	[29]
11	$CH_2 + OH \rightarrow CH + H_2O$	1.13×10^{7}	2.0	3000	[29]
12	$CH_2 + M'' \rightarrow$ products	1.0×10^{13}	0.0	0	[29]
13	$CH + M' \rightarrow$ products	3.0×10^{13}	0.0	0	[29]

parameter for the present flames which remain globally mixing controlled.

Figures 4–8 present comparisons between the measured and predicted radial profiles of local mean gas temperature and gas species concentrations (O_2, CO_2, C_3H_8 and CO) for flame A, respectively. Identical comparisons for flames B and C may be found in Meunier [28]. On the whole the quality of the predictions is fairly good, except near the burner region where the flame width and the fuel concentrations are overpredicted. It is also evident that the mathematical model predicts a faster conversion of CO to CO_2 than that observed experimentally.

Figures 9 and 10 show the measured axial profiles of local mean NO_x concentrations and equivalence ratios for flames A, B and C, respectively. The equivalence ratio in *Figure 10* represents the ratio between the measurements of local mean C_3H_8 and O_2 concentrations, divided by the same ratio at stoichiometry, which may be viewed as the local equivalence ratio of combustion products. It can be observed (*Figure 9*) that the NO_x concentration rapidly increases downstream from the injector tip, reaching a maximum at $x/d_0 = 50$ for flames A and B and $x/d_0 = 100$ for flame C. At these positions the concentration of UHC is significant (fuel-rich region), as indicated by the local value of the equivalence ratio of the combustion products (*Figure 10*). This observation reveals that the prompt mechanism may be the dominant formation path for NO in the present flames. In fact, it is well accepted [1–4,31] that the prompt mechanism is initiated by fast reactions between N_2 and hydrocarbon radicals leading to the formation of HCN. The

Table 3 Summary of the initial conditions

Flame	d_0 (mm)	u_0 (m/s)	Re[a]	Fr[a]
A	4.15	12.32	11440	3730
B	3.25	11.05	8030	3830
C	2.05	25.25	11580	31730

[a] Based on cold fuel properties

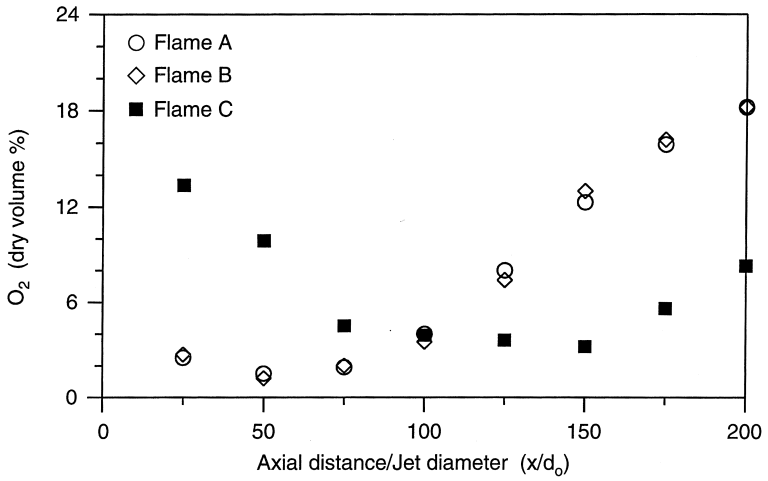

Figure 2 Measured axial profiles of mean O_2 concentrations for flames A, B and C

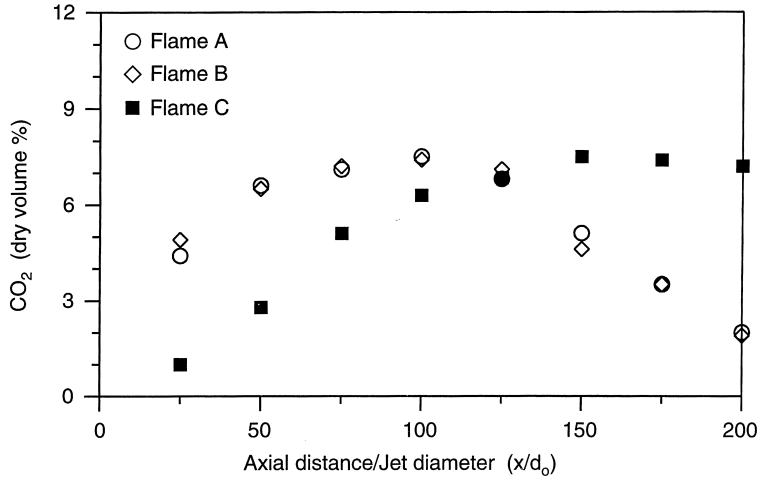

Figure 3 Measured axial profiles of mean CO_2 concentrations for flames A, B and C

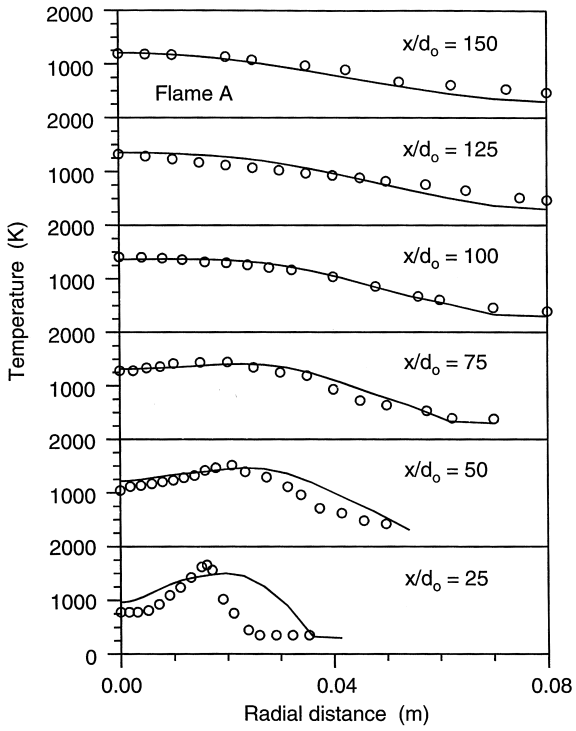

Figure 4 Measured and predicted radial profiles of mean gas temperatures for flame A (symbols: measurements; solid line: predictions)

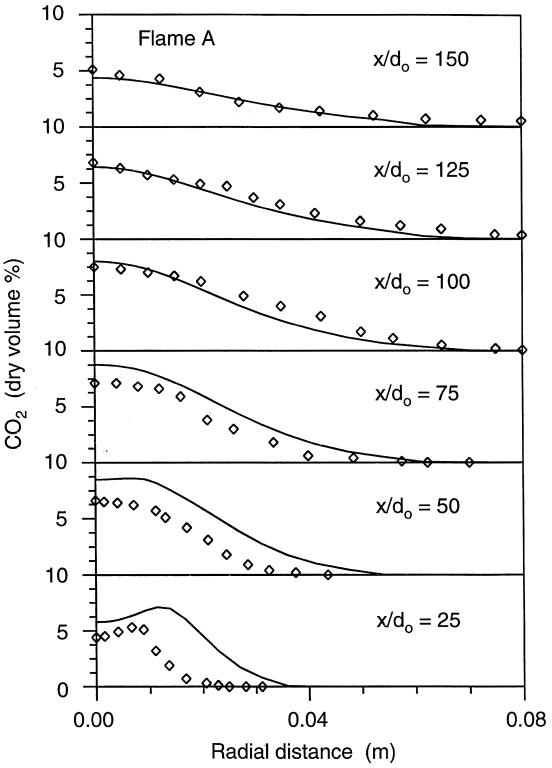

Figure 6 Measured and predicted radial profiles of mean CO_2 concentrations for flame A (symbols: measurements; solid line: predictions)

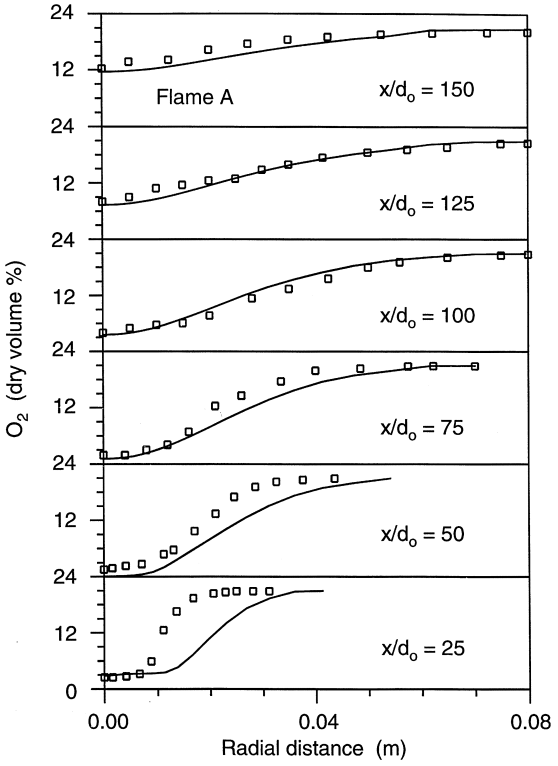

Figure 5 Measured and predicted radial profiles of mean O_2 concentrations for flame A (symbols: measurements; solid line: predictions)

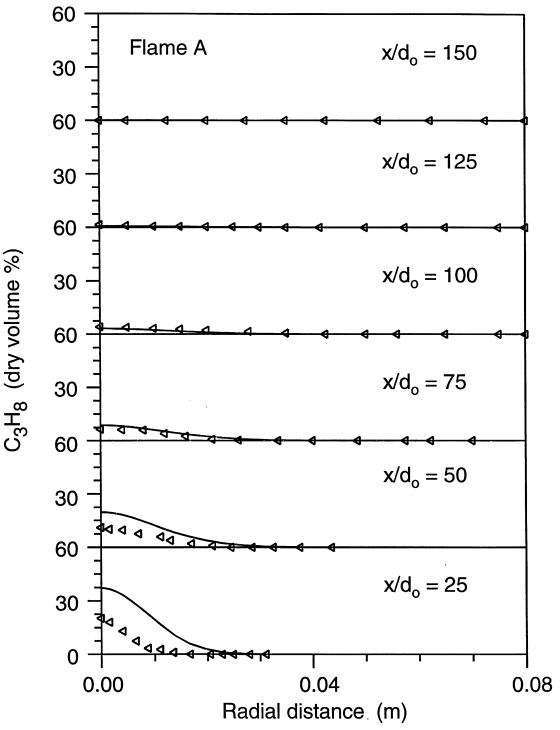

Figure 7 Measured and predicted radial profiles of mean C_3H_8 concentrations for flame A (symbols: measurements; solid line: predictions)

major contribution comes from CH [1]:

$$CH + N_2 \rightarrow HCN + N \quad (10)$$

In previous measurements carried out in turbulent propane diffusion flames by Buriko and Kuznetsov [32], the NO_x concentration maximum was found to lie in the leaner region of the flame while Takagi *et al.* [33] observed that NO is likely to form in the narrow region corresponding to the flame front where the gas temperature is maximum and in the region not far from the fuel nozzle. However, in all studies, NO concentration quickly reaches a marked peak which seems to confirm the importance of the prompt mechanism.

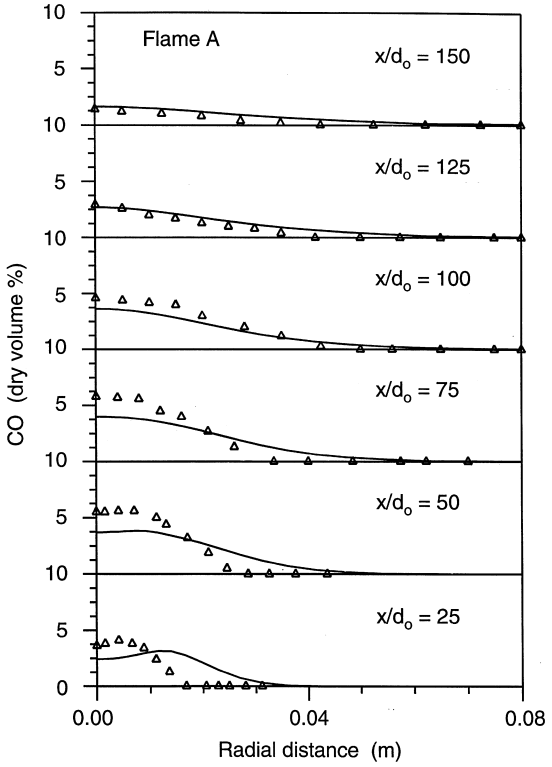

Figure 8 Measured and predicted radial profiles of mean CO concentrations for flame A (symbols: measurements; solid line: predictions)

Figures 9 and 10 also show that the NO_x concentration starts decreasing in fuel-rich regions where the concentration of UHC is still significant. In the case of flames A and B, for example, the NO peak occurs at about $x/d_0 = 50$ while the stoichiometry in the combustion products is only reached at $x/d_0 = 125$. This result suggests that reactions converting NO to N_2 through reactions with hydrocarbon radicals may therefore play an important role in the nitrogen chemistry of the present flames. Under rich combustion conditions, there is the possibility of reaction between NO and hydrocarbon free radicals, leading to the formation of hydrogen cyanide and eventually of molecular nitrogen [1,3,5,34]. The main reaction paths in converting NO to N_2 through HCN and CN are supposed to be due to the following reactions [1]:

$$CH_i + NO \rightarrow HCN + H_{i-1}O \quad (11)$$

$$HCCO + NO \rightarrow HCNO + CO \quad (12)$$

Reaction (12) was also added to the reaction scheme of Glarborg *et al.* [27] as described above in the presentation of the mathematical model.

Figures 11 and 12 compare the measured and predicted radial profiles of local mean NO_x concentrations using the three models (thermal, prompt and global) for flames A and C, respectively. Identical comparisons for flame B [28] are similar to those presented for flame A. *Figures 11 and 12* show that the predictions obtained using the thermal mechanism clearly underestimate the experimental data. Moreover, the position of the calculated NO peaks indicates that the thermal mechanism cannot reproduce the experimental trends. The maximum calculated NO concentrations are found in the last stages of the flame ($x/d_0 = 125$ and 150 for flame A) while the measured NO peaks are observed in the first stages of the flame ($x/d_0 = 50$ and 75 for flame A). The thermal mechanism cannot therefore be the dominant path for NO formation.

Figures 11 and 12 show predictions of in-flame NO concentrations for both flames A and C obtained with the prompt NO model using Williams *et al.*'s constants [35] but keeping the oxygen reaction order as initially proposed by De Soete:

$$\frac{dX_{NO}}{dt} = kfX_{O_2}^{b}X_{N_2}X_{fuel}^{0.024}\exp\left(-\frac{60\,000}{RT}\right) \quad (13)$$

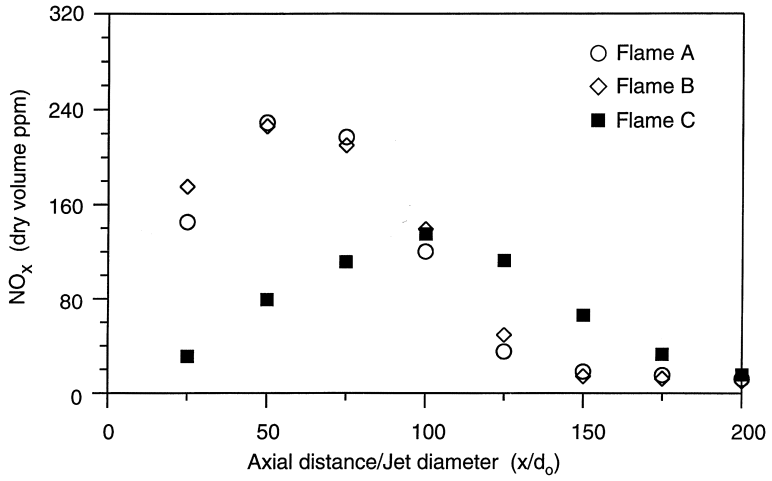

Figure 9 Measured axial profiles of mean NO_x concentrations for flames A, B and C

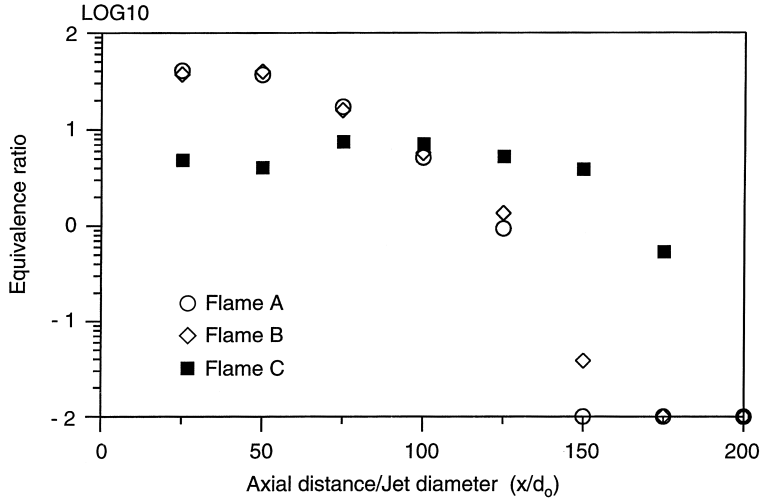

Figure 10 Measured axial profiles of mean fuel equivalence ratios for flames A, B and C

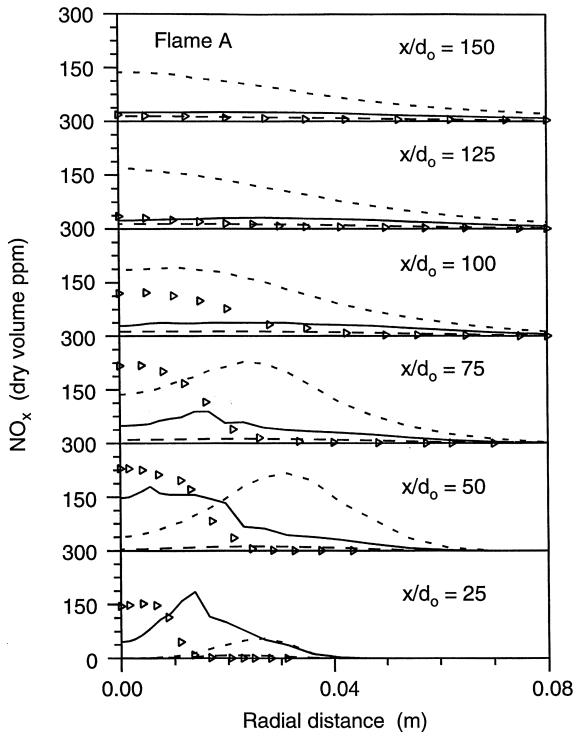

Figure 11 Measured and predicted radial profiles of mean NO_x concentrations for flame A (symbols: measurements; solid line: global NO mechanism; — — —: thermal NO mechanism; - - -: prompt NO mechanism)

The prompt formation rate expressions initially proposed by de Soete [15] and later modified by Williams and co-workers [14,35] failed to predict the NO peak by at least one order of magnitude. These predictions are not presented here. The NO concentration is underpredicted using de Soete's expression and is overpredicted using Williams *et al.*'s expression.

Eqn (13) provides a faster and greater NO formation rate than that of the thermal model. However, *Figures 11 and 12* indicate that the experimental and the prompt numerical profiles strongly diverge in shape. Although the peak value of predicted NO concentration is in reasonable agreement with the experimental peak for flame A, this is not the case for flame C where the experimental NO peak is about two times greater than the predicted one. Moreover, the predictions fail to reproduce the NO decrease, which is clearly observed for flame A for axial locations beyond 100 diameters.

Finally, the solid lines in *Figures 11 and 12* represent the calculations using the global NO mechanism. The global NO concentration results, despite not being completely satisfactory, present for both flames a fast increase in NO concentration in the first stages of the flame followed by a strong reduction to reach the measured NO concentration level at the end of the combustion region. These numerical results seem to confirm our early interpretation of the experimental data, indicating that the prompt NO mechanism is dominant in the NO formation and that the reactions between NO and fuel radicals play an important role in the nitrogen chemistry of hydrocarbon flames. As previously described for laminar methane flames with the Miller and Bowman scheme [6–8], the present model predicts a very large NO formation by the prompt NO mechanism but also a very large NO reduction by fast reburn reactions (CH_i + NO and HCCO + NO). Neglecting these last reactions would provide a strong overprediction of NO concentrations.

In general, the reasonable agreement between the NO predictions and experimental data suggests that a good estimate of the NO concentration field in turbulent diffusion flames can be achieved using the flamelet concept and reduced reaction schemes for combustion and relevant nitrogen chemistry. This agreement is less satisfactory at the station $x/d_0 = 25$. This results mainly from the inadequate predictions of the gas temperatures and major species concentrations as illustrated in *Figures 4–8*. The other sources of discrepancies between the experimental data and the predictions can be attributed mostly to the limitation of the present turbulence/NO chemistry modelling and to the limitations in the simplified reaction mechanisms chosen for propane combustion. An alternative [36] would be to obtain the concentration of the minor species needed to determine the formation and oxidation rates of NO and HCN from flamelet calculations rather than from steady-state assumptions.

CONCLUSIONS

The main purpose of the work reported here was to study the specific chemical routes for the formation and destruction of NO in turbulent propane diffusion flames. To this end,

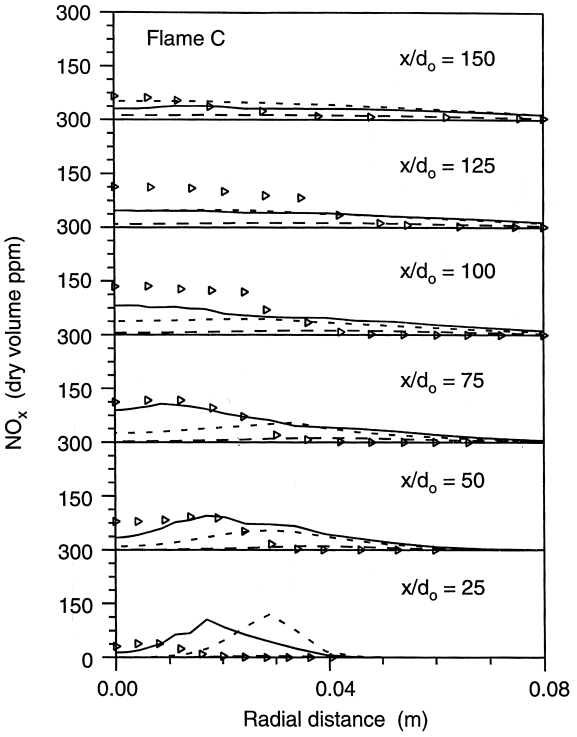

Figure 12 Measured and predicted radial profiles of mean NO_x concentrations for flame C (symbols: measurements; solid line: global NO mechanism; — — —: thermal NO mechanism; - - -: prompt NO mechanism)

detailed in-flame measurements of local mean gas temperature and local mean gas species concentrations of O_2, CO, CO_2, UHC and NO_x, for three flames, have been analysed with the aid of a mathematical model. In the numerical NO calculations, a relevant nitrogen chemistry scheme, which included both thermal and prompt NO formation as well as NO to HCN recycling and the conversion of HCN to NO or N_2, has been compared with both the Zeldovich reactions and a global prompt NO reaction scheme. The main conclusions of this study are that: (1) the prompt NO mechanism is the dominant route for the NO formation; and (2) the reactions between NO and hydrocarbon radicals, recycling NO to HCN via the fuel NO reactions, play an important role in the global NO reduction.

ACKNOWLEDGEMENTS

This work was partially supported by the Mobility Program of the Commission of the European Communities, Grant No. JOU2-923010. The authors would like to thank Dr. de Soete for his help in the discussion of the results. The authors would also like to thank Mr. Jorge Coelho for his help in preparing the figures.

REFERENCES

1 Miller, J. A. and Bowman, C. T., *Progress in Energy and Combustion Science*, 1989, **15**, 287.
2 Bowman, C. T., in *Twenty-Fourth Symposium (International) on Combustion*. The Combustion Institute, 1992, p. 859.
3 De Soete, G. G., *Revue Générale de la Thermique*, 1989, **330**, 353.
4 Drake, M. C. and Blint, R. J., *Combustion and Flame*, 1991, **83**, 185.
5 Mitchell, R. E., Nitrogen oxide formation in laminar methane–air diffusion flames. Ph.D. Thesis, Massachusetts Institute of Technology, 1975.
6 Nishioka, M., Kondoh, Y. and Takeno, T., in *Twenty-Sixth Symposium (International) on Combustion*. The Combustion Institute, 1996, p. 2139.
7 Hewson, J. C. and Bollig, M., in *Twenty-Sixth Symposium (International) on Combustion*. The Combustion Institute, 1996, p. 2171.
8 Smyth, K. C., *Combustion Science and Technology*, 1996, **115**, 151.
9 Peters, N. and Donnerhack, S., in *Eighteenth Symposium (International) on Combustion*. The Combustion Institute, 1981, p. 33.
10 Turns, S. R., *Progress in Energy and Combustion Science*, 1995, **21**, 361.
11 Chen, R. Y. and Driscoll, J. F., in *Twenty-Third Symposium (International) on Combustion*. The Combustion Institute, 1991, p. 281.
12 Turns, S. R. and Myhr, F. H., *Combustion and Flame*, 1991, **87**, 317.
13 Al-Fawaz, A. D., Dearden, L. M., Hedley, J. T., Missaghi, M., Pourkashanian, M., Williams, A. and Yap, L., in *Twenty-Fifth Symposium (International) on Combustion*. The Combustion Institute, 1994, p. 1027.
14 Missaghi, M., Pourkashanian, M., Williams, A. and Yap, L., in *Proceedings of the American Flame Foundation Conference*, USA, 1990.
15 De Soete, G. G., in *Fifteenth Symposium (International) on Combustion*. The Combustion Institute, 1975, p. 1093.
16 Meunier, Ph., Costa, M. and Carvalho, M. G., *Combustion and Flame*, 1998, **112**, 221.
17 Liew, S. K., Bray, K. N. C. and Moss, J. B., *Combustion and Flame*, 1984, **56**, 199.
18 Sanders, J. P. H. and Lamers, A. P. G. G., *Combustion and Flame*, 1994, **96**, 22.
19 Liew, S. K., Bray, K. N. C. and Moss, J. B., Flamelet modelling of chemical closures in turbulent propane–air combustion. Report TP-84-81, School of Mechanical Engineering, Cranfield Institute of Technology, UK, 1984.
20 Kent, J. H. and Bilger, R. W., in *Sixteenth Symposium (International) on Combustion*. The Combustion Institute, 1976, p. 1643.
21 Abou Ellail, M. M. M., Gosman, A. D., Lockwood, F. C. and Megahed, I. E. A., *Journal of Energy*, 1982, **2**, 71.
22 Coelho, P. and Carvalho, M. G., *Journal of Engineering for Gas Turbines and Power*, 1996, **118**, 887.
23 Lockwood, F. C. and Shah, N. G., in *Eighteenth Symposium (International) on Combustion*. The Combustion Institute, 1981, p. 1405.
24 Truelove, J. S., A mixed grey gas model for flame radiation. Report HL76/3448/KE, AERE Harwell, UK, 1976.
25 Khan, I. H. and Greeves, G., in *Heat Transfer in Flames*, ed. N. Afgan and J. M. Béer, 1974, p. 391.
26 Magnussen, B. and Hjertager, B. H., in *Sixteenth Symposium (International) on Combustion*. The Combustion Institute, 1976, p. 719.
27 Glarborg, P., Lilleheie, N. I., Byggstoyl, S., Magnussen, B. F., Kiplinen, P. and Huppa, M., in *Twenty-Fourth Symposium (International) on Combustion*. The Combustion Institute, 1992, p. 889.
28 Meunier, Ph., A theoretical and experimental study on nitric oxide in turbulent diffusion flames. Ph.D. Thesis, Université Catholique de Louvain, Belgium, 1996.
29 Rokke, N. A., Hustad, J. E., Sonju, O. K. and Williams, F. A., in *Twenty-Fourth Symposium (International) on Combustion*. The Combustion Institute, 1992, p. 385.
30 Patankar, S. V., *Numerical Heat Transfer*, 1981, **4**, 409.
31 Matsui, Y. and Nomaguchi, T., *Combustion and Flame*, 1978, **32**, 205.
32 Buriko, Y. Y. and Kuznetsov, V. R., *Combustion, Explosion and Shockwaves*, 1978, **14**, 296.

33 Takagi, T., Ogasawara, M., Fujii, K. and Daizo, M., in *Fifteenth Symposium (International) on Combustion*. The Combustion Institute, 1975, p. 1051.
34 Miller, J. A., Branch, M. C., McLean, W. J., Chandler, D. W., Smooke, M. D. and Kee, R. J., in *Twentieth Symposium (International) on Combustion*. The Combustion Institute, 1984, p. 673.
35 Williams, A., Wolley, R. and Lawes, M., *Combustion and Flame*, 1992, **89**, 157.
36 Lentini, A., Potentialities of the stretched laminar approach for turbulent combustion. *International Symposium on Turbulence, Heat and Mass Transfer*, Paper 7, Lisbon, Portugal, 1994.